atmosphere

MDPI

Article

Analysis of the Sporadic-E Layer Behavior in Different American Stations during the Days around the September 2017 Geomagnetic Storm

Laysa C. A. Resende [1,2,*], Yajun Zhu [1], Christina Arras [3], Clezio M. Denardini [2], Sony S. Chen [2], Juliano Moro [1,4], Diego Barros [2], Ronan A. J. Chagas [2], Lígia A. Da Silva [1,2], Vânia F. Andrioli [1,2], José P. Marchezi [1,2], Alexander J. Carrasco [2], Chi Wang [1], Hui Li [1] and Zhengkuan Liu [1]

[1] State Key Laboratory of Space Weather NSSC/CAS, Beijing 100190, China
[2] National Institute for Space Research—INPE, São José dos Campos 12227-010, Brazil
[3] Department 1—Geodesy and Remote Sensing, German Research Centre for Geosciences (GFZ), Helmholtz Centre Potsdam, 14473 Potsdam, Germany
[4] Southern Space Coordination—COESUL, Santa Maria 97105-900, Brazil
* Correspondence: laysa.resende@inpe.br

Abstract: The development of sporadic-E (Es) layers over five Digisonde stations in the American sector is analyzed. This work aims to investigate the dynamic of such layers during the days around the geomagnetic storm that occurred on 8 September 2017. Therefore, a numerical model (MIRE) and Radio Occultation (RO) technique are used to analyze the E layer dynamics. The results show a downward movement in low-middle latitudes due to the wind components that had no significant changes before, during, and after the geomagnetic storm. In fact, our data and simulations showed weak Es layers over Boulder, Cachoeira Paulista, and Santa Maria, even though the winds were not low. However, the RO data show the terdiurnal and quarterdiurnal influence in the Es layer formation, which can explain this behavior. In addition, we observed an atypical Es layer type, slant Es layer (Es_s), during the main phase of the magnetic storm over Boulder. The possible cause of the Es_s layers was gravity waves. Another interesting point is the spreading Es layer occurrence associated with the Kelvin–Helmholtz Instability (KHI). Finally, it is confirmed that the disturbed electric field only influenced the Es layer dynamics in regions near the magnetic equator.

Keywords: sporadic-E (Es) layer; tidal winds; geomagnetic storm

Citation: Resende, L.C.A.; Zhu, Y.; Arras, C.; Denardini, C.M.; Chen, S.S.; Moro, J.; Barros, D.; Chagas, R.A.J.; Da Silva, L.A.; Andrioli, V.F.; et al. Analysis of the Sporadic-E Layer Behavior in Different American Stations during the Days around the September 2017 Geomagnetic Storm. *Atmosphere* **2022**, *13*, 1714. https://doi.org/10.3390/atmos13101714

Academic Editors: Chen Zhou and Zhibin Yu

Received: 25 September 2022
Accepted: 13 October 2022
Published: 18 October 2022

1. Introduction

The denser layers in the E region, 100–140 km, are known as Sporadic (Es). They are characterized by being thin, occurring in different formats that are classified in letters in digital ionosonde data. These letters refer to the physical mechanism of the Es layer development, and it has three main categories (Es_b, Es_q, and Es_b). The blanketing Es layers (Es_b) are due to the wind shear mechanisms, which occur in magnetic latitudes around ±20–60° [1]. The equatorial Es layers (Es_q), related to Gradient Drift instabilities (or Type II irregularities), are characterized by diffuse and non-blanketing Es trace in ionograms acquired around ±5° [2]. The third type, known as auroral layers (Es_a), is associated with electric fields and particle precipitation and occurs over the poles [3]. Additionally, within the Es_b layers, we have other classifications: "c" (cusp, Es_c), "h" (high, Es_h), and "l (low, Es_l)/f" (flat, Es_f). In addition, we have the s (slant, Es_s) type that are attributed to the presence of gravity waves [4].

The components of the tidal winds (diurnal, semidiurnal, terdiurnal, and quarterdiurnal) are the main agents responsible for the Es dynamics at low and middle latitudes. This process, the wind shear mechanism, is characterized by wind components carrying the ions in opposite directions. Due to the magnetic field presence, there is a Lorentz force

making the molecular (N_2^+, NO^+, O^+, O_2^+) and metallic ions (Fe^+, Mg^+, Ca^+, Na^+) move upward or downward [1]. Thus, in the null points of these winds, there is an accumulation of these ions forming a new layer. The electrons follow the magnetic field lines to maintain neutrality in the plasma, allowing the Es layer duration [5]. For this reason, wind shear is ineffective around the magnetic equator [6].

There are doubts about the relationship between geomagnetic magnetic storm occurrences and Es layer development. In fact, the role of the electric field is negligible at low and middle latitudes [7]. Ref. [8] affirmed that in regions with a magnetic inclination angle higher than 2°, the electric field plays only a small role in the formation of the Es layers. Therefore, the wind shear mechanism is predominant in the Es layer formation in these latitudes [1]. Some authors also mention that the tidal winds do not suffer from the magnetic storms event [9], although this subject is still under discussion.

Recently, ref [2,10] discovered some interesting Es layer behavior at low latitudes due to magnetic storms. They observed strong Es layers are a consequence of the combined effect of the winds and disturbed electric fields. In fact, the westward disturbed electric field due to the disturbance dynamo effect (DDEF) caused an intensification in the Es layer in regions near the geographical equator, where the winds have low velocity. Additionally, the Gradient Drift instability due to the Equatorial Electrojet Current (EEJ) can intensify during a magnetic storm main phase, mainly due to the prompt penetration electric fields (PPEFs) action [11–14], and the Es_q layer is observed in low latitudes stations. The authors also observed that the disturbed electric field has no influence in regions far away from the magnetic equator.

Additionally, in low and middle latitudes, atypical and multiple Es layers are seen in Digisonde data that is associated with the Kelvin–Helmholtz Instability (KHI) [15]. The KHI is caused by the large wave amplitudes caused by the winds. In fact, suitable differences between the ion and electron mobilities can cause an unstable ambient, forming large wave amplitudes. This instability can be seen through the spreading in the Es layer [16]. Other interesting results were found by [17], revealing multiple Es layer traces associated with the influence of the electric fields. In such work, the authors analyzed the electron density, the electric field, and wind components in the E region heights during the SEEK-2 rocket campaign on 3 August 2002. Their results showed that the complex Es structures observed in the ascending phase of the SEEK-2 rocket launching could be due to the electric field. The authors suggested that the electric field causes a convergence in the ions into a layer at several altitude regions, contributing to the Es layer formation. However, [17] they do not mention the electric field's source. They only mention that this electric field component had an external origin and that it was possibly generated by an F-region disturbance. In addition, the KHI appeared to be unrelated to the magnetic storm events.

Therefore, the impact of geomagnetic storms in Es layer development over equatorial and low-middle latitudes is still discussed in the literature. Until now, we do not know the real effect on the physical mechanisms of the Es layer formation during disturbed periods. To analyze this behavior in depth, we analyzed the observed Es layer from five Digisondes stations over the American sector, Boulder (40.6° S, 105° W, dip ~50°), Jicamarca (12° S, 76.8° W, dip ~0.5°), São Luís (2.3° S, 44.2° W, dip ~8°), Cachoeira Paulista (22.7° S, 45° W, dip ~35°), and Santa Maria (29.7° S, 53.8° W, dip ~−37°),during the geomagnetic storm of 8 September 2017. The ionospheric parameters presented several interesting behaviors on days before, during, and after the storm. We also examined the Es layer behavior using a numerical model MIRE (Portuguese acronym for E Region Ionospheric Model) and Radio Occultation (RO) technique. This analysis confirmed that wind shear was the principal agent of the Es layer formation over low and middle latitudes [1,7,10]. Finally, this study aims to investigate the dynamic of the Es layers during the days around the geomagnetic storm that occurred on 8 September 2017, to investigate the differences in their dynamics.

2. Data Analysis and Methodology

2.1. The Es Layer Parameters Obtained in Ionograms

The electron density and virtual height of the Es layer are obtained in ionograms provided by Digisonde, which is a high-frequency radar with a variable operational frequency of 1 to 20–30 MHz. This equipment consists of a transmitter, receiver, and antennas [18], and it is widely used to analyze the Es layer. In this work, we used a chain of Digisondes (Figure 1) at Boulder (BOU), Jicamarca (JIC), São Luís (SLZ), Cachoeira Paulista (CXP), and Santa Maria (SMS). The magnetic equator from the International Geomagnetic Reference Field (IGRF) model is shown as the red line for the year 2017. The white circles refer to the South America Magnetic Anomaly (SAMA) position, a region with a low magnetic field intensity.

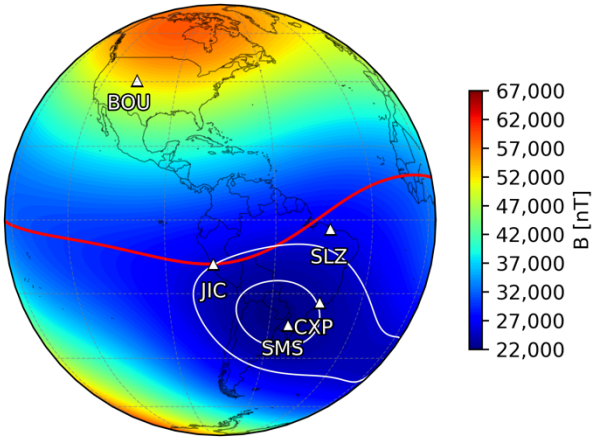

Figure 1. Map showing the instrument sites used in this study. The magnetic equator positions in 2017 (red line) and the SAMA location (white isolines) are also shown. The acronyms for the stations are: BOU, Boulder; JIC, Jicamarca; SLZ, São Luís; CXP, is Cachoeira Paulista; SMS, Santa Maria.

The parameters analyzed here are the blanketing frequency (*fb*Es), which refers to the frequency at which reflections from a layer at greater heights may be observed, and the virtual height of the Es layer (*h'*Es). The *fb*Es is associated with the electron density through the relationship: n = 1.24 × 10^4 (*fb*Es)^2 [19]. In addition, the ionograms are taken between 5, 10, or 15 min, depending on the location.

2.2. MIRE Mode8

The theoretical model (MIRE) is used to analyze the physical mechanism in the Es layer formation. MIRE provides the E and Es electron density using the continuity and momentum differential equations for the molecular/atomic (NO^+, O_2^+, N_2^+, O^+) and metallic (Fe^+, Mg^+) ions, varying from 86 to 120 km in a step of 0.05 km to height, and from 00 LT to 24 LT in a step of 2 min to time [20,21]. All the details about this model can be found in [20] and [22].

In MIRE, the basic equation to analyze the Es layer dynamic is the ions' vertical velocity given in Equation (1).

$$V_{iz} = \frac{\omega_i^2}{(v_{in}^2+\omega_i^2)}[\cos I \cdot \sin I \cdot U_X + \frac{v_{in}}{\omega_i} \cdot \cos I \cdot U_y + \frac{1}{v_{in}} \frac{e}{m_i} \cdot \cos I \cdot \sin I \cdot E_x + \frac{e}{\omega_i m_i} \cdot \cos I \cdot E_y + \frac{e}{v_{in} m_i} \cdot (\frac{v_{in}^2}{\omega_i^2} + sin^2 I) \cdot E_z] \quad (1)$$

where ω_i is the ion gyrofrequency, v_{in} is the ion-neutral collision frequency, I is the magnetic inclination angle, m_i is the ion mass, e is the ion electric charge, E_x, E_y, and E_z are the electric field components, and U_x is the meridional and U_y is the zonal wind components. The following reference system represents all the vectors: the X-axis points towards the

south, and the Y-axis points to the east, whereas the Z-axis completes the right-handed coordinate system, pointing up.

Thus, it is possible to choose the scenario to simulate the Es layer dynamics, winds, and/or electric fields. After that, MIRE calculates the ion density for each component, considering all the chemical reactions and their coefficients that can be found in [20]. The electron density (*ne*) is acquired through the charge neutrality conditions using the sum of the concentrations of the molecular/metallic ions (Equation (2)):

$$ne = \left[O_2^+\right] + \left[NO^+\right] + \left[O^+\right] + \left[N_2^+\right] + \left[Fe^+\right] + \left[Mg^+\right]. \quad (2)$$

2.3. The Winds Profile

The wind profile here is obtained using the Global Scale Wave Model (GSWM-00) (http://www.hao.ucar.edu/modeling/gswm/gswm.html, accessed on 3 September 2022), which successfully describes the atmospheric tides wind dynamics for the altitudes analyzed in this work [19,20].

The wind profile here is obtained in the Global Scale Wave Model (GSWM-00) (http://www.hao.ucar.edu/modeling/gswm/gswm.html, accessed on 3 September 2022), which successfully describes the wind dynamics at low heights [23,24]. The GSWM-00 outputs zonal and meridional; diurnal (24 h) and semidiurnal (12 h) amplitudes and phases are included in the wind shear equations given in Equations (3) and (4) for the correspondent latitude of each analyzed station.

$$U_x(z) = U_{x0}(z) \cdot cos\left(\frac{2\pi}{\lambda_x}(z - z_0) + \frac{2\pi}{T}(t - t_{x0}(z))\right), \quad (3)$$

$$U_y(z) = -U_{y0}(z) \cdot sin\left(\frac{2\pi}{\lambda_y}(z - z_0) + \frac{2\pi}{T}(t - t_{y0}(z))\right), \quad (4)$$

where $U_{x0}(z)$ and $U_{y0}(z)$ correspond to wind magnitudes at the height z, λ_x and λ_y are the wavelengths, T is the tidal period (24 h for diurnal and 12 h for semidiurnal), z_0 is a reference height, assumed as 100 km, and $t_{x0}(z)$ and $t_{y0}(z)$ are the wave phases.

2.4. The Es Layer Detection by Radio Occultation (RO) Technique

A multi-satellite constellation of LEO (low Earth orbit) is widely used to sound the atmosphere on a global scale using the GPS radio occultation (RO) technique [25]. During a GPS radio occultation, the Earth's atmosphere is scanned between the LEO orbit altitude and the Earth's surface. In fact, the LEO satellite observes a modification in the GPS signal that is related to the refractive index of the atmosphere. Thus, it is possible to obtain atmospheric parameters such as temperature, pressure, electronic density, and others. In addition, the main LEO satellite missions that provide GPS RO data are CHAMP (Challenging Minisatellite Payload), GRACE (Gravity Recovery and Climate Experiment), and FORMOSAT-3/COSMIC (FORMOsa SATellite mission-3/Constellation Observing System for Meteorology, Ionosphere, and Climate). These missions have accumulated an extensive database with an expressive number of RO profiles available. Refs. [25,26] describe more details about this technique.

Therefore, the GPS RO technique can detect the Es layer (blanketing Es layers) using the signal-to-noise ratio (SNR) profiles described in [26]. In fact, the strong fluctuations in SNR represent the Es layer occurrence, and it is a good technique for analyzing the Es layer behavior around the globe [27,28]. These fluctuations are detected numerically by applying a bandpass filtering technique. The SNR profiles are normalized, and the standard deviation (SD) is calculated for the whole profile in a 2.0 km running window. Thus, when the SD exceeds a numerically defined threshold and the fluctuation in the profile has an altitude range lower than 10 km, we consider an Es layer detection. It is important to mention here that the atmosphere is scanned with a 50 Hz rate down to the

surface to allow analyzing the thin structures that are the Es layers, and for this reason, it is not possible to study this profile above 120 km.

Lastly, we analyze the S4 index using the RO technique in this work. The degree of the SNR fluctuation can be obtained and is related to the intensity of the Es layer, called the S4 scintillation index.

3. Results

3.1. The 8 September 2017, Geomagnetic Storm

We used the Dst index to identify the geomagnetic storm periods, and it chose the quiet periods. This data was acquired from the World Data Center in Kyoto (http//wdc.kugi.kyoto-u.ac.jp/dstae/index.html, accessed on 1 August 2022). We analyzed on days around the geomagnetic storm driven by the Interplanetary Coronal Mass Ejection (CME) that occurred on 7 September 2017.

Figure 2 shows: (a) the variations of the Dst index in nT, (b) the solar wind velocity in km/s (V_R), (c) the number density of protons per cm^3 (N_P), (d) the Bz component of the interplanetary magnetic field (IMF) in nT, and (e) the AE index. The interplanetary medium parameters were obtained from the Magnetic Field Experiment (MAG) and Proton and Alpha Monitor (SWEPAM) instruments onboard the Advanced Composition Explorer (ACE) spacecraft [29]. The vertical black lines refer to the beginning of the sudden commencement, the main phase, and the recovery phase of the geomagnetic storm.

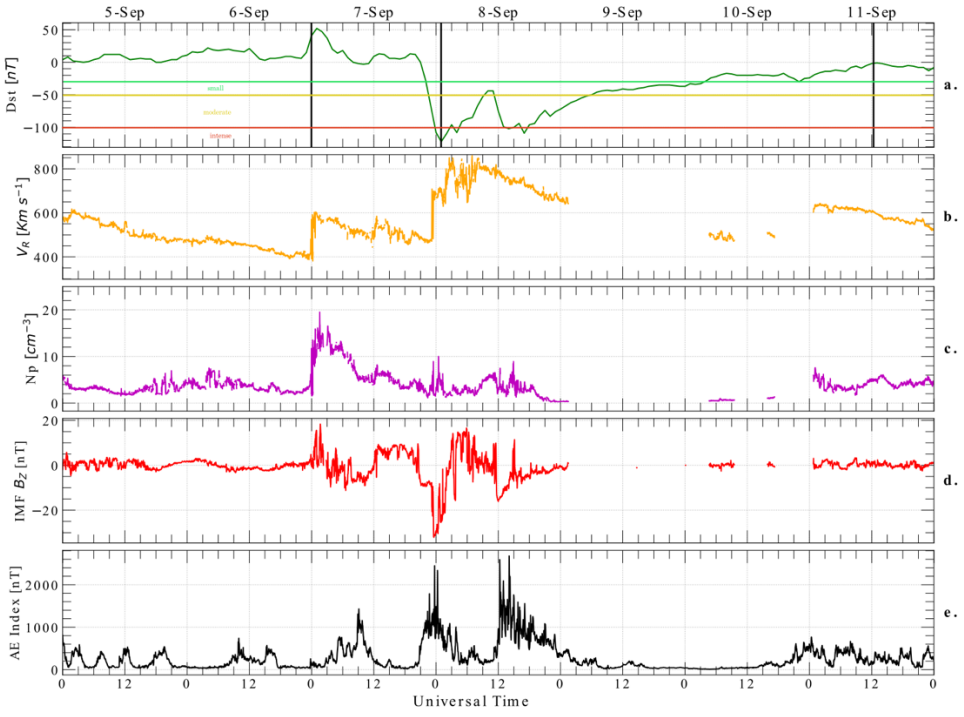

Figure 2. (**a**) The Dst index; (**b**) the solar wind velocity V_R; (**c**) the number density of protons N_P; (**d**) the interplanetary magnetic field component Bz; and (**e**) the AE index from 5–11 September 2017.

The CME arrived in the Earth's magnetosphere at 2300 UT on 7 September 2017, causing an abrupt increase in the Bz component. The CME effect lasted until 9 September 2017, at around 0100 UT. In this period, the Bz component turned southward (negative). After that, the Earth's environment started to recover. The Dst index reached −122 nT at 0200 UT on 8 September 2017, which is considered an intense storm according to the classification by [30]. The V_R increased gradually from about 400 km/s to around 800 km/s. Furthermore, the AE index showed values higher than 2000 nT on 7 September. The recovery phase started on 8 September 2017, in which the parameters returned gradually to typical behavior.

3.2. The Behaviour of the Es Layer Parameters over the American Sector

In this work, we evaluate the electronic density of the *fb*Es and the *h'*Es over the American sector. Figure 3 shows the *fb*Es between 5–11 September 2017 (red symbols) from top to bottom: Boulder, São Luís, Jicamarca, Cachoeira Paulista, and Santa Maria. The vertical line refers to the magnetic storm onset. Notice that there were no available data in Cachoeira Paulista, which are marked as "No Data". The main characteristic we observed was a cosine behavior in all stations, showing a pattern of enhancement starting at around 0900 UT, reaching maximum values at around 1200 UT, followed by a steady decrease [20].

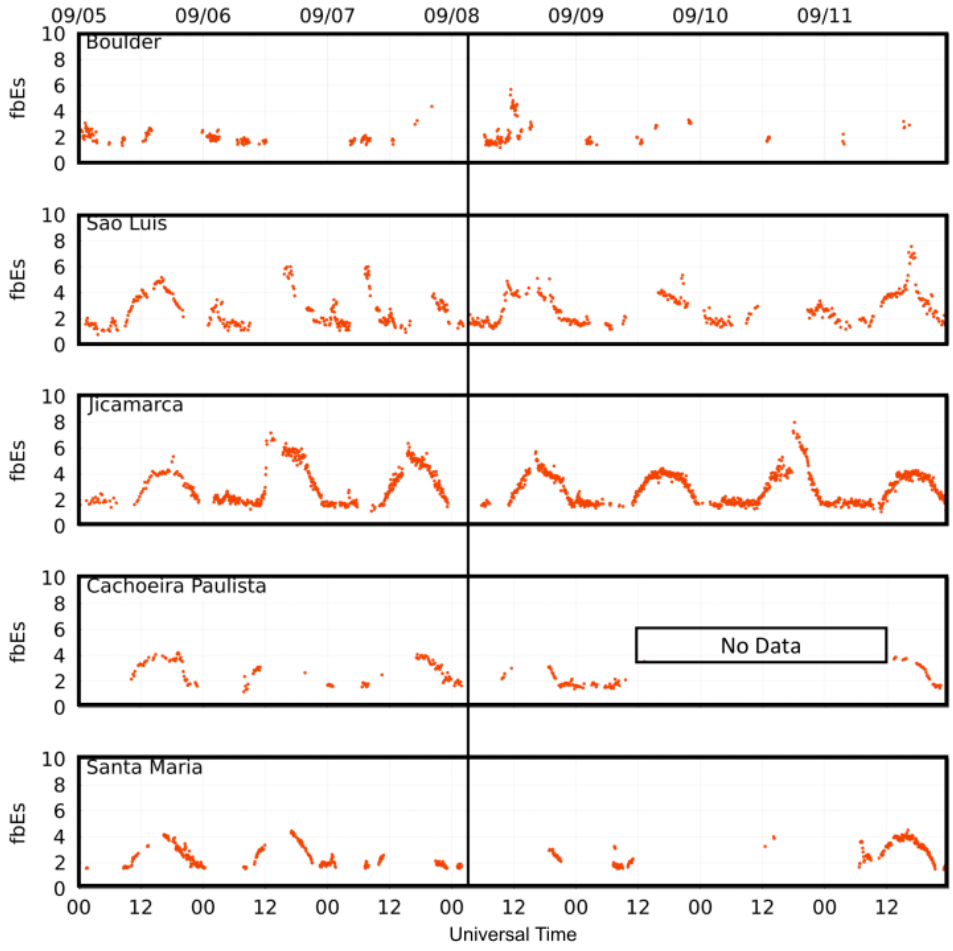

Figure 3. The *fb*Es parameter (red symbols) from top to bottom: Boulder, São Luís, Jicamarca, Cachoeira Paulista, and Santa Maria on 5–11 September 2017.

The *fb*Es did not reach values greater than 6 MHz on most days, except in short hours during daytime over Jicamarca. We also observed a peak in São Luís on 11 September (around 1600–1700 UT), in which the *fb*Es reached almost 8 MHz. It is important to mention that the Jicamarca station is located at equatorial latitudes in South America. Consequently, the Es layers over this station do not block the upper regions (Es_q layers), and the *fb*Es refer to the minimum F layer trace (*fmim*F).

Another feature was the absence of the Es layer over all stations. This fact is associated with the M and X solar flare occurrences during the days studied [31–33]. On 6 September 2017, the solar flare class reached X9.3, and at all the stations, we did not observe the Es layer for some hours (starting around 0800 UT). The X-ray from the solar flare significantly increased the ionization of the D region, causing radio signal absorption through this layer. This behavior is called blackout, and when it occurred, the Es layer and F region traces were partially or totally not observed [5,34].

Figure 4 presents the virtual height of the Es layer using the *h*′Es parameter between 5–11 September 2017 (green symbols) from top to bottom: Boulder, São Luís, Jicamarca, Cachoeira Paulista, and Santa Maria. The literature [1,20,26] shows that the Es layer height at low-mid latitudes varied between 90 and 150 km. In addition, these Es layers moved downward due to the tidal winds [4]. The exception was Jicamarca, where the Es_q layer (an irregularity layer) was located around 95–100 km. The dashed lines refer to the downward movement of the Es layer at low and middle latitudes, and the black and red lines are related to the days before, during, and after the magnetic storm occurrence, respectively. In some hours, the height had values greater than 150 km, indicating the presence of intermediate layers [35].

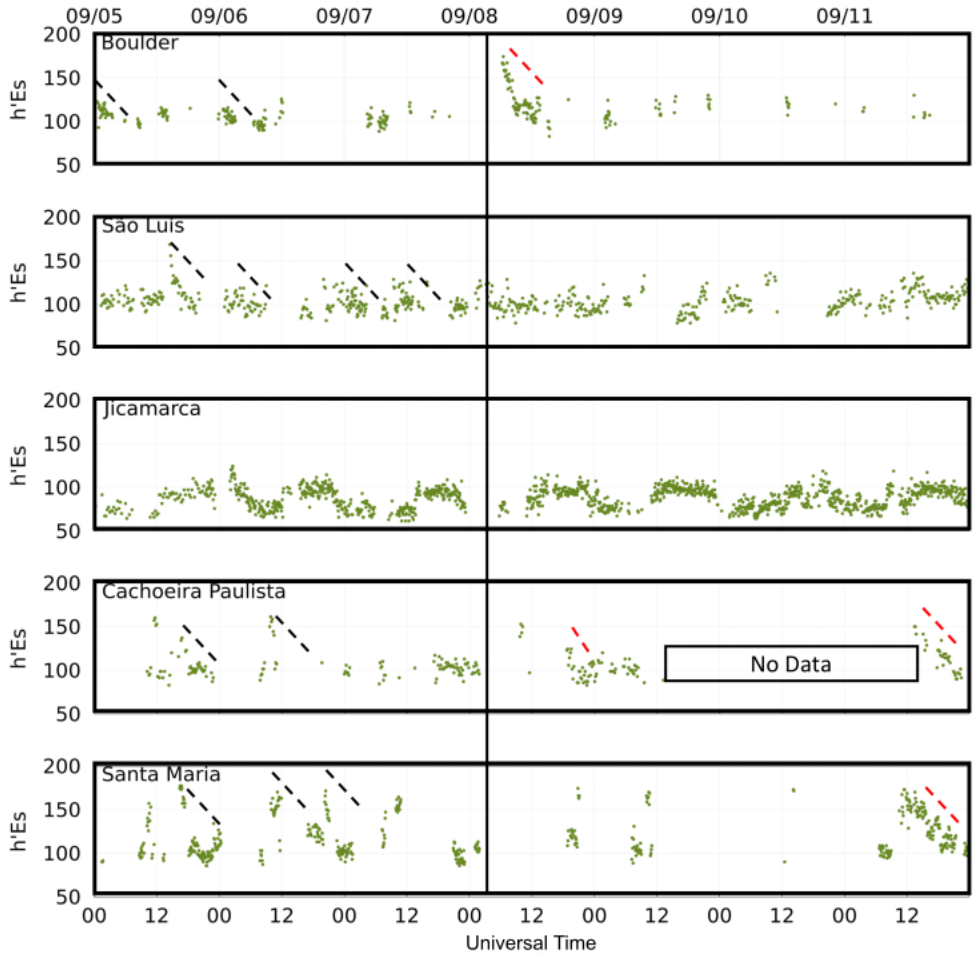

Figure 4. The *h*′Es parameter (green symbols) from top to bottom: Boulder, São Luís, Jicamarca, Cachoeira Paulista, and Santa Maria on 5–11 September 2017. The dashed lines refer to the downward movement of the Es layer at low and middle latitudes, and the black and red lines are related to the days before, during, and after the magnetic storm occurrence, respectively.

Therefore, the main points observed are:

(1) In general, the Es layer development had no significant changes over Cachoeira Paulista and Santa Maria in the days that preceded and during the geomagnetic storms;
(2) In São Luís, we observed steady Es layers located around 100 km. This pattern is the same as the Es layer behavior over Jicamarca;
(3) The high Es layers occurred a few moments after the start of the magnetic storm over Boulder due to the presence of the "s" type (slant) (dashed red lines); and
(4) The atypical spreading Es layer was observed over Boulder and Santa Maria.

All these points will be discussed in the following section.

4. Discussion

4.1. The Physical Dynamic in the Es Layer Development over the American Sector

Before, during, and after the magnetic storm, the Es layer performed a downward movement shown in *h'*Es (dashed lines in Figure 4). This behavior was due to the tidal winds dynamic, in which the diurnal and semidiurnal tides act in the Es layer. Figure 5 shows some ionograms illustrating the Es layer movement over: (a) Boulder, (b) Cachoeira Paulista, and (c) Santa Maria. Analyzing these ionograms, we observed the intermediate Es layer presence occurrence (layers located around 150–180 km) when the dynamic was controlled by the winds, diffusion, and molecular ions. At these heights, we had the low amplitudes of the zonal wind, the absence of the metallic ions, and the high ambipolar plasma diffusion coefficient value, making the intermediate layers last only a short time. In fact, these layers tend to perform a downward movement due to the semidiurnal action in a time interval of a few minutes to hours, forming Es_c or Es_l types [36]. In middle latitudes, such as Boulder and Santa Maria (transition stations between the low-and mid-latitudes), the wind amplitudes tend to be stronger than equatorial and low-latitudes stations [10]. For this reason, the Es_h seems to last longer than at Cachoeira Paulista.

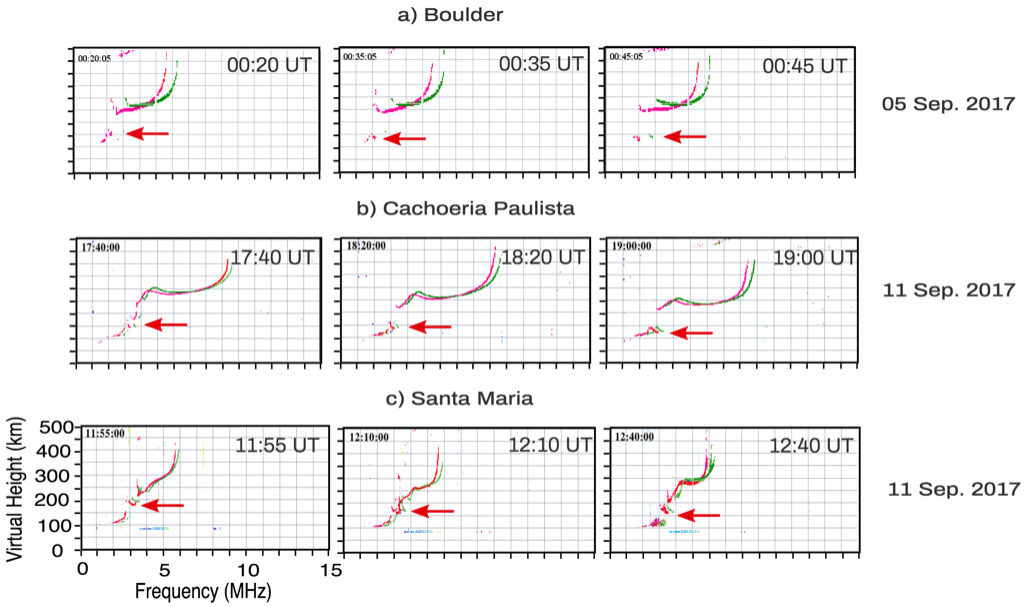

Figure 5. Ionograms collected at: (**a**) Boulder; (**b**) Cachoeira Paulista; and (**c**) Santa Maria show the downward movement due to the wind action.

We used a MIRE for the regions analyzed to verify the wind pattern in such regions. Figure 6 shows the meridional (left panel) and the zonal (middle panel) wind components obtained using GSWM for Boulder (Figure 6a), Cachoeira Paulista (Figure 6b), and Santa Maria (Figure 6c). It is important to mention that the GSWM-00 tidal winds are monthly. Thus, we chose September to simulate the Es layer. In addition, the wind components considered here are diurnal and semidiurnal. The zero curves in the wind profiles refer to the shear responsible for the Es layer occurrence in simulations. The zonal components have strong amplitudes concerning the meridional winds in the three locations analyzed. The right panel of Figure 6 presents the Height–Time–Intensity (HTI) maps of the electron density in a log scale simulated by MIRE. In the background of these simulations, we have the E region density, characterized by the low and high electron density values in the nighttime and daytime, respectively. In all stations, we observed thin layers that refer to the Es layers.

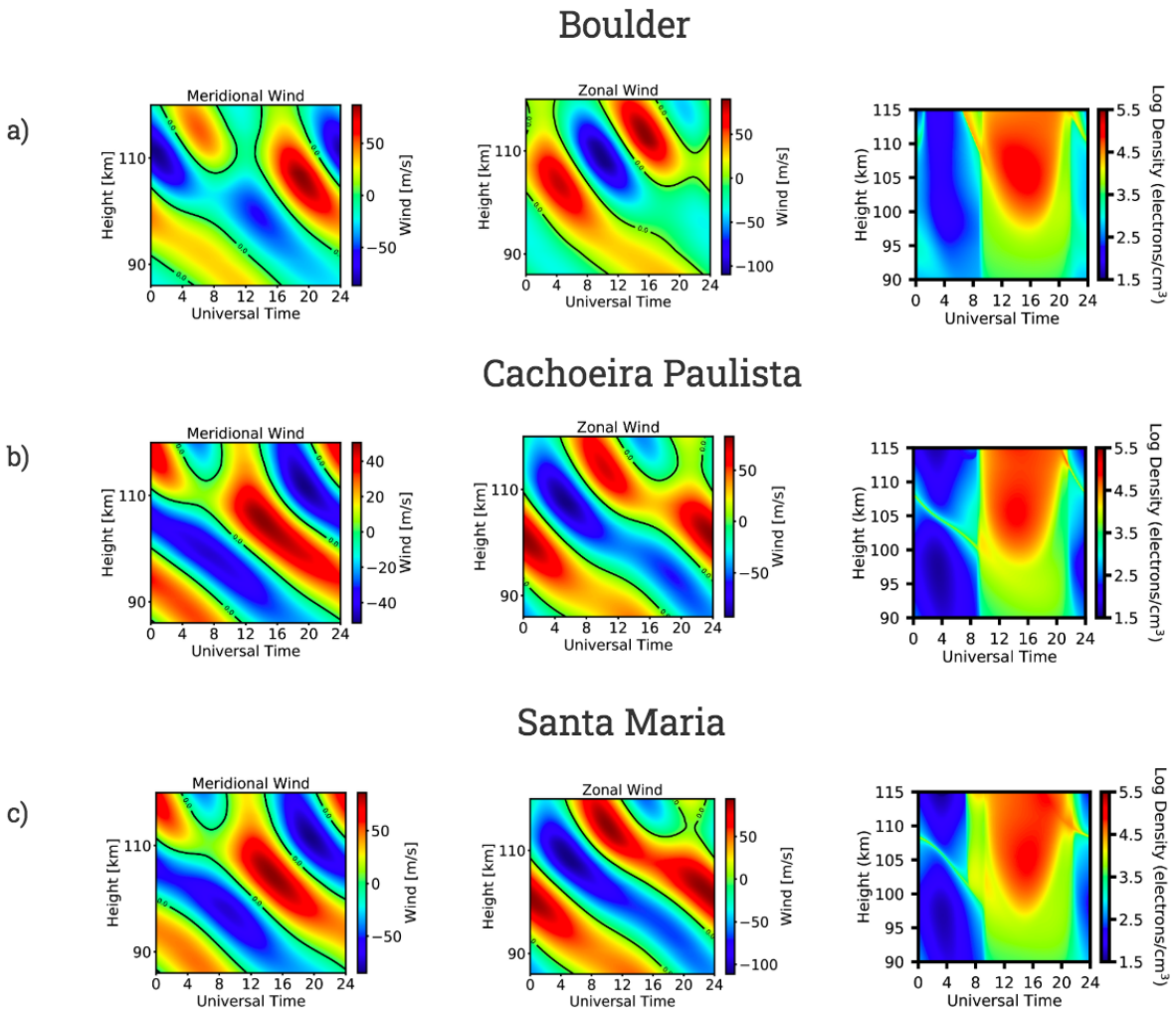

Figure 6. Wind profile of the meridional (left panel) and zonal (middle panel) components obtained using GSWM and electron density (right panel) as a function of Universal Time (UT) and height (km) simulated by MIRE considering the diurnal and semidiurnal tidal winds representative of September 2017 for: (**a**) Boulder; (**b**) Cachoeira Paulista; and (**c**) Santa Maria.

The Es layers in the simulations are related to the wind components, i.e., the denser layers classified by "c", "f", or "l" types. Unfortunately, our simulations were up to 115 km, and it was not possible to analyze the Es_h layers. However, notice that the results present a downward movement for the three low-middle regions analyzed here, agreeing with the observational data shown in Figure 4. One important point is that the Es layer in simulations is weak during nighttime for the three stations compared to other previous works using MIRE for low latitudes [20].

The diurnal and semidiurnal tides in the mesosphere and lower thermosphere (MLT) region are the main components that control the Es layer dynamics [1]. In addition, it is believed that the electric fields do not cause any modification in the Es layer development [36]. However, other components, such as terdiurnal and quarterdiurnal, can also act in the Es layer formation. MIRE does not consider these components because we do not have available data or models. Thus, to verify this behavior, we analyzed a global visualization of the Es layer density using the RO technique based on the constellation of LEO (low Earth orbit) satellite data. The LEO satellite missions that provide RO data are FORMOSAT/COSMIC (FORMOsa SATellite mission/Constellation Observing System for Meteorology, Ionosphere, and Climate). This mission has accumulated an extensive database to study the Es layers [26]. The signal-to-noise ratio (SNR) profiles were used to

identify the Es layer through RO since they are sensitive to abrupt changes in the electron density in the ionosphere. The SNR showed strong fluctuations when passing a sporadic E layer. The authors in [26] give details about this detection. The S4 (scintillation) index is a method to estimate the intensity of the Es layer using the sampling point, which is assumed to be the altitude of the Es layer [28]. The S4 refers to the intensity of the Es layer.

Therefore, Figure 7 shows the S4 scintillation index in the latitude range of 80° to 80° south and north in September in 2017. This graph refers to the global distribution of GPS RO profiles provided by the COSMIC satellites. All the days that the Es layer occurred were considered. The disadvantage of this data mode is that we do not obtain information above ~120 km. Thus, the numbers of the Es layer considered were very low concerning the Digisonde data. The color bars show the S4 index varying between 0 and 0.30. Notice a clear tidal signature around −20° and 20° when the Es layer intensity was more expressive. In addition, we noted that the Es layer was very weak in Northern middle latitudes, agreeing with the observational data and simulations over Boulder. The main observation in the RO result is the quarterdiurnal signature at Southern low latitude stations, whereas the semidiurnal is seen at the Northern. Ref. [37] analyzed the quarterdiurnal tide influence in the Es layer development in a middle latitude station. The results show that during the equinoxes, the zonal wind shear is an important driving mechanism for the quarterdiurnal in the Es layer, even their amplitudes being low. Thus, it is interesting that the Es layer dynamics at low and middle latitudes are controlled by the tide wind behavior only, independent of the disturbance occurrences.

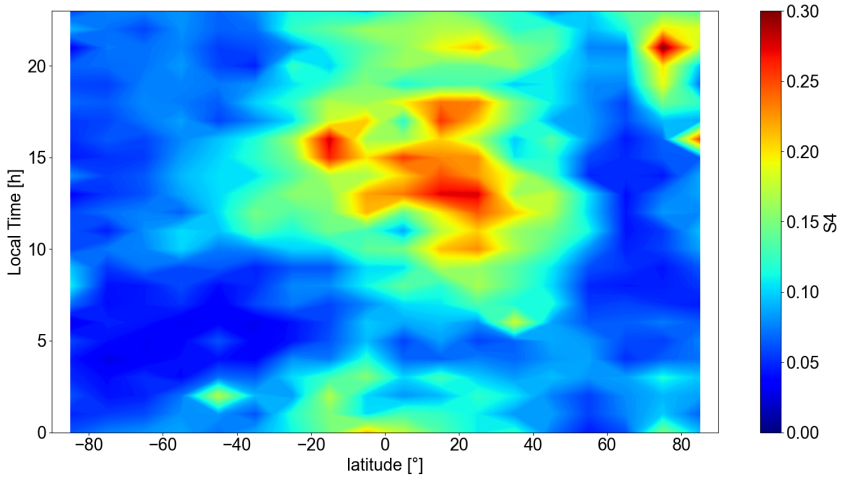

Figure 7. The S4 scintillation index in the latitude range of 80° to 80° south and north in September 2017.

Thus, we did not observe significant changes in the Es layer during the disturbed periods for Boulder, Cachoeira Paulista, and Santa Maria. We verified the simulations for days before the main phase of the magnetic storm (not shown here), and we did not see any considerable differences. In fact, the disturbed electric fields can influence the Es layer structures during geomagnetic storms in stations where the wind has low amplitudes [30]. The electric field induced by the prompt penetration electric fields (PPEFs) or due to the disturbance dynamo effect (DDEF) when it is directly westward can cause an intensification in the Es layer, as seen in Equation (1). However, as we have seen in the weak Es layers with the maximum *fb*Es of 5 MHz and in the simulations, the winds controlled all the Es layer dynamics, and electric fields did not cause any modification in the Es layer development, agreeing with the hypothesis in [38].

There was only one effect mechanism due to the magnetic storms that occurred over Santa Maria, which was the auroral Es (Es_a) layer occurrence in ionograms, similar to the auroral sites. Santa Maria is a station located in the center of the South America Magnetic Anomaly (SAMA), as shown in Figure 1, characterized by the low magnetic field intensity value. Thus, it is possible to have particle precipitation mechanisms, and although the Es_a

layers are not expected in stations outside of the polar regions, they can occur over Santa Maria [39]. In our time study, we saw the Es_a during the recovery phase on 9 September 2017 (not shown here). Other works [3] and [39] also saw the Es_a layers in recovery over the SAMA regions. Therefore, it is well established that such layers happened because of the low-energy electron precipitation over the SAMA region. Generally, when the Es_a signatures occur, the winds have a secondary role in the Es layer development, and it is difficult to detect these Es layer types in the ionograms.

Regarding the equatorial regions, it is well-known that the Equatorial Electrojet (EEJ), an eastward electric current during the daytime driven by the zonal and vertical electric fields, causes plasma instabilities in the E region [5]. These instabilities, named Gradient Drift, are responsible for the Es_q layers in ionograms, characterized by a diffuse and non-blanketing trace located at 100 km [40]. This explains the stable behavior in the *h*′Es over Jicamarca (Figure 4). In fact, the wind shear was not effective due to the horizontal configuration of the magnetic field, not allowing the denser/blanketing layer formation [10].

Over São Luís, we had an interesting behavior that was the competition between the winds and electric field in Es layer development [6]. The geomagnetic field configuration is different in the Brazilian sector, with a high declination compared to other equatorial regions. The magnetic inclination angle varies at a rate of 20′ per year, corresponding to an apparent northwestward movement of the magnetic equator at a rate of 11.6′/year [41]. Thus, as analyzed by [5] and [42] it is possible to observe the Es layer types due to the winds and the Es_q layer due to the EEJ instabilities over São Luís. This behavior was common until 2015. After this year, the magnetic equator is not located near São Luís, and the Es_q layer is not always seen anymore.

However, ref [2] found evidence that distant regions of the magnetic equator can also experience such equatorial dynamics during disturbed periods. In such analysis, they investigated the Es layer development in regions not so close to the magnetic equator during a High-Speed Solar Wind Stream (HSS) event. Using the Digisonde and magnetometer data and simulations, the authors observed the expansion of the EEJ current and, consequently, the instability occurrences. Therefore, the wind shear, mainly during the main magnetic storm phase, does not affect the boundary equatorial magnetic sites. Consequently, the Es_q layers occurred in São Luís. Figure 8 shows the ionograms over (a) Jicamarca and (b) São Luís during the main magnetic storm phase. Notice that the Es_q layer, which is always predominant over Jicamarca, occurred over São Luís.

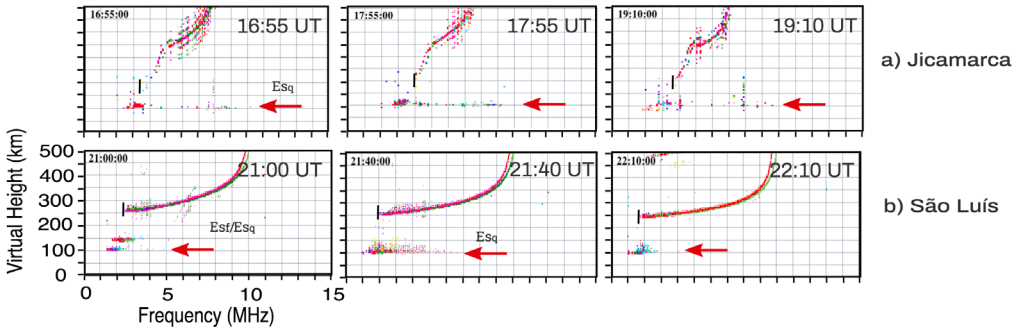

Figure 8. Ionograms collected at: (**a**) Jicamarca: and (**b**) São Luís during the main geomagnetic storm phase, showing the Es_q layer presence in both stations.

The event analyzed here refers to a CME, and it is known that the ionospheric responses concerning the HSS are different. The previous results in [2] show Es_q layers during the main phase of the magnetic storm only, and during the recovery phase, the EEJ current weakened, allowing the winds to play a role in the Es layer formation again. Nevertheless, we notice that the Es layer pattern in electron density and height dynamics (Figures 3 and 4) show similarities between Jicamarca and São Luís. In fact, the ionograms over São Luís (not shown here) during the days after the magnetic storm showed weak Es

layers. The winds started to act only on 11 September, in which strong blanketing of Es layers was observed in São Luís data, as seen in the *fb*Es peak for this station in Figure 3. Thus, we believe that during intense geomagnetic storms, this EEJ expansion has a longer duration, an impossibility with the action of the winds in the Es layer development during the recovery geomagnetic storm phase [43,44].

4.2. The Gravity Wave Role in the Es Layer Development over Boulder during the Main Magnetic Storm Phase

An interesting behavior in this study was that the Es_s layer presence over Boulder was characterized by the oblique propagation of the radio signal. Figure 9 shows some ionograms illustrating the Es layer types (red arrows) during the *fb*Es peaks over Boulder on 8 September 2017. The black line in the left panel shows the *fb*Es localization. Although this parameter refers to the minimum point of the region above the Es layer, sometimes this layer is so strong that we use the maximum point in the second reflection of such an Es layer. In addition, it is possible to see that the Es_s occurred between 10:55 UT and 11:55 UT. Interestingly, the Es_s layer occurred right after the magnetic storm onset.

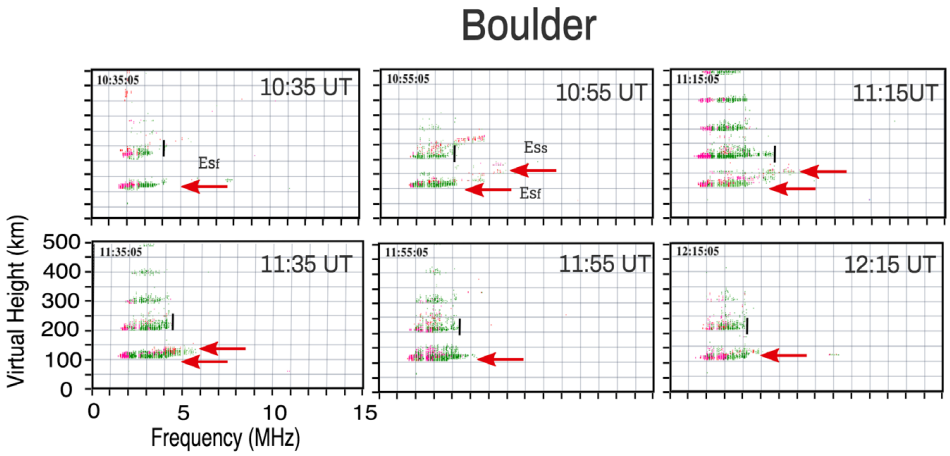

Figure 9. Ionograms collected at Boulder during the main geomagnetic storm phase show the Es_s layer and Es_f spreading, associated with the gravity waves and the Kelvin–Helmholtz Instability, respectively.

Additionally, the Es_s layer trace was due to the atmospheric gravity waves (AGW), or it may have been associated with the presence of irregularities embedded in the E [45]. It is not expected in low and middle latitudes regions [36]. This layer always appears with other Es layer types, generally "q" or "f/l". The Es_f occurred at the same time as the Es_s layer. Notice that the Es_f spread, reaching values that did not exceed 4 MHz.

The influence of gravity waves in the Es layer development is still a topic of study, mainly during disturbed times. Ref. [46] affirmed that the atmospheric gravity waves could form the Es layer since these wave structures caused a node in the vertical drift velocity, allowing the accumulations of the metallic ions (mainly Fe^+). In addition, [38] observed that the atypical Es layers over middle latitude stations in China are associated with the gravity wave presence. Ref. [45] noted the Es_s layer presence in some hours over Brazilian stations. However, they do not deeply analyze the physical proprieties of these occurrences.

Hence, we have evidence that the Es_s layer that can occur in ionograms during a magnetic storm's main phase may be due to the gravity wave action. Furthermore, an interesting characteristic that caught our attention is that the flat trace was very spread. As mentioned before, Ref. [47] affirmed that wind instabilities can cause the Es_s layer also. Some works mentioned that the Kelvin–Helmholtz Instability (KHI) could source atypical Es layers in middle latitudes [11]. According to [47], the gravity wave excitation by unstable shears with large amplitudes caused a growth of the KHI instability. These authors also affirmed that KH instability is among the most common sources of turbulence. Thus, we

believe that the KH instability excited the gravity waves, and this is an explanation for the spread of Es_f and Es_s layer occurrences over Boulder during the disturbed time.

Finally, we find an interesting behavior over Santa Maria on 5 September 2017, days before the geomagnetic storm. We notice the same spreading trace that we observed over Boulder, as is possibly seen in the ionograms of Figure 10. Nevertheless, these atypical Es layers occurred during nighttime. Although this layer is similar to "a" type, it occurred in a quiet period, being unlike the action of particle precipitation. Here, we believed that it was evidence that the high amplitudes of the winds observed over Boulder and Santa Maria can cause instabilities over these middle latitude stations. This fact requires further investigation with more data to be fully understood. However, our results indicate that the wind dynamics are the only factor responsible for the development and atypical Es layer occurring in both quiet and disturbed periods over low and middle latitudes.

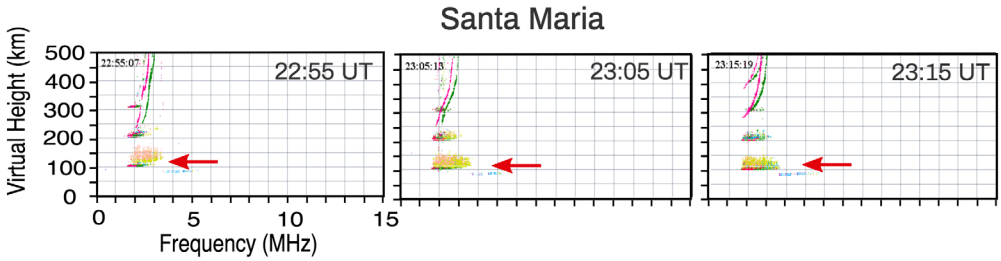

Figure 10. Ionograms collected at Santa Maria on 5 September 2017, showing the atypical Es layer in this station.

5. Conclusions

We presented a study about the Es layer dynamics during days around a geomagnetic storm that occurred on 8 September 2017. We analyzed the five Digisonde stations over the American sector to verify the Es layer behavior. We also used MIRE and RO data simulations to observe the wind influence on the dynamics of the Es layer during quiet and disturbed periods.

In general, the Es layer development had no significant changes over low and middle latitudes in the days preceding and during the geomagnetic storms. We saw the downward movement during the days before the magnetic storm due to the wind dynamics. In some hours, the height of the Es layers had values greater than 150 km, meaning the intermediate layers were present. The simulations agreed with this descendent movement of the Es layer in the ionograms.

One important point is that the Es layer in simulations was weak during nighttime for Boulder, Cachoeira Paulista, and Santa Maria. Analyzing the S4 index in the RO data, we observed that the Es layer was very weak in the Northern middle latitudes, agreeing with the observational data and simulations over Boulder. In addition, the main observation in the RO result was the quarterdiurnal signature in the Es layer formation at Southern low latitude stations, whereas the semidiurnal was seen at the Northern. This behavior is an interesting finding, showing that the Es layer dynamics at low and middle latitudes are controlled by the tidal winds only, independent of the disturbance occurrences.

Over São Luís, we observed steady Es layers located around 100 km. This pattern agrees with the Es layer behavior over Jicamarca. We observed that the Es_q layers developed during the main and recovery phases of the geomagnetic storm in the boundary equatorial magnetic site, São Luís. This result confirms that Gradient Drift instability can intensify during disturbed periods, extending the EEJ influence to these border regions. However, in the previous works in the literature, the Es_q layer was not observed days after the main phase of the magnetic storm.

The high Es layers occurred a few moments after the start of the magnetic storm over Boulder due to the presence of the "s" type (Es_s). Hence, we have evidence that the gravity waves acted in the Es layer development. Another interesting characteristic is the spreading Es layer trace seen in the Es_s simultaneously. Some works in the literature mentioned that

the Kelvin–Helmholtz Instability (KHI) could cause these atypical Es layers in middle latitudes. The same spreading Es layer was observed over Santa Maria on 5 September 2017, days before the geomagnetic storm. Here, we believed that it was evidence that the high amplitudes of the winds observed over Boulder and Santa Maria can cause instabilities over these middle latitude stations. This fact requires further investigation with more data to be fully understood.

Finally, our results indicate that the wind dynamics are the only response to the development and atypical Es layer that occurred in quiet and disturbed periods over low and middle latitudes.

Author Contributions: Data curation, L.C.A.R., J.M., C.A., S.S.C., R.A.J.C., J.P.M. and L.A.D.S.; formal analysis, L.C.A.R., C.M.D., Y.Z., V.F.A. and J.M.; funding acquisition: C.W.; investigation, L.C.A.R., J.M., A.J.C. and D.B.; methodology, L.C.A.R., J.M., C.A. and A.J.C., Project administration, Z.L. and H.L.; supervision, C.M.D. and Y.Z., visualization, L.C.A.R. and R.A.J.C.; writing—original draft, L.C.A.R.; writing—review and editing, L.C.A.R. All authors have read and agreed to the published version of the manuscript.

Funding: This work was supported by the International Partnership Program of Chinese Academy of Sciences, Grant No. 183311KYSB20200003 and 183311KYSB20200017.

Institutional Review Board Statement: Not applicable.

Informed Consent Statement: Not applicable.

Data Availability Statement: The authors used the OMNIWeb (https://omniweb.gsfc.nasa.gov/form/dx1.html, accessed on 1 August 2022) for the interplanetary medium parameters at the L1 Lagrangian point, WDC Kyoto (http://wdc.kugi.kyoto-u.ac.jp/aeasy/index.html, accessed on 1 August 2022) for the provisional AE and Dst index, and the NOAA National Centers for Environmental Information (NCEI) for the magnetic equator from IGRF-13 (https://www.ngdc.noaa.gov/geomag/calculators/magcalc.shtml#igrfgrid, accessed on 1 August 2022). The Digisonde data can be downloaded upon registration at the Embrace webpage from INPE Space Weather Program in the following link: http://www2.inpe.br/climaespacial/portal/en/, accessed on 24 September 2022.

Acknowledgments: L.C.A. Resende would like to thank the China-Brazil Joint Laboratory for Space Weather (CBJLSW), National Space Science Center (NSSC), Chinese Academy of Sciences (CAS) for supporting her postdoctoral (Grant No. 183311KYSB20200003 and 183311KYSB20200017). Y. Zhu, C. Wang, H.Li and Z. Liu thanks the CBJLSW/NSSC/CAS. C.M. Denardini thanks CNPq/MCTI, respectively, by grant 303643/2017-0. J. Moro would like to thank the CBJLSW/NSSC/CAS for supporting his postdoctoral, and the CNPq/MCTIC (grant 429517/2018-01). S.S. Chen thanks CAPES/MEC (grants 88887.694874/2022-00 and 88887.362982/2019-00). V.F.A., L.A. Da Silva, and J.P.M. would like to thank the CBJLSW/NSSC/CAS for supporting their postdoctoral. R.A.J. Chagas, and A. J. Carrasco thanks the INPE.

Conflicts of Interest: The authors declare no conflict of interest.

References

1. Haldoupis, C. A tutorial review on Sporadic E layers. *Aeron. Earth's Atmosph. Ionos.* **2011**, *29*, 381–394.
2. Resende, L.C.A.; Zhu, Y.; Denardini, C.; Batista, I.S.; Shi, J.; Moro, J.; Chen, S.S.; Conceição-Santos, F.; Da Silva, L.A.; Andrioli, V.F.; et al. New Findings of the Sporadic E (Es) Layer Development Around the Magnetic Equator During a High-Speed Solar (HSS) Wind Stream Event. *J. Geophys. Res.* **2021**, *126*, e2021JA029416. [CrossRef]
3. Batista, I.S.; Abdu, M.A. Magnetic storm associated delayed sporadic E enhancements in the Brazilian Geomagnetic Anomaly. *J. Geophys. Res.* **1977**, *82*, 4777–4783. [CrossRef]
4. Conceição-Santos, F.; Muella, M.T.A.H.; Resende, L.C.A.; Fagundes, P.R.; Andrioli, V.F.; Batista, P.P.; Carrasco, A.J. On the role of tidal winds in the descending of the high type of sporadic layer (Esh). *Adv. Space Res.* **2020**, *65*, 2131–2147. [CrossRef]
5. Resende, L.C.A.; Denardini, C.M.; Batista, I.S. Abnormal fbEs enhancements in equatorial Es layers during magnetic storms of solar cycle 23. *J. Atmos. Terr. Phys.* **2013**, *102*, 228–234. [CrossRef]
6. Resende, L.C.A.; Batista, I.S.; Denardini, C.M.; Carrasco, A.J.; Andrioli, V.F.; Moro, J.; Batista, P.P.; Chen, S.S. Competition between winds and electric fields in the formation of blanketing sporadic E layers at equatorial regions. *Earth Space Sci.* **2016**, *68*, 201. [CrossRef]
7. Whitehead, J.D. Recent Work on Mid-Latitude and Equatorial Sporadic-E. *J. Atmos. Terr. Phys.* **1989**, *51*, 401–424. [CrossRef]

8. Dagar, R.; Verma, P.; Napgal, O.; Setty, C.S.G.K. The relative effects of the electric fields and neutral winds on the formation of the equatorial sporadic layers. *Ann. Geophys.* **1977**, *33*, 333–340.
9. Prasad, S.N.V.S.; Prasad, D.S.V.V.D.; Venkatesh, K.; Niranjan, K.; Rama Rao, P.V.S. Diurnal and seasonal variations in sporadic E-layer (Es layer) occurrences over equatorial, low and mid latitude stations—A comparative study. *Indian J. Radio Space Phys.* **2012**, *41*, 26–38.
10. Resende, L.C.A.; Shi, J.; Denardini, C.M.; Batista, I.S.; Picanço, G.A.; Moro, J.; Chagas, R.A.J.; Barros, D.; Chen, S.S.; Nogueira, P.A.B.; et al. The Impact of the Disturbed Electric Field in the Sporadic E (Es) Layer Development Over Brazilian Region. *J. Geophys. Res.* **2021**, *126*, e2020JA028598. [CrossRef]
11. Yamazaki, Y.; Richmond, A.; Maute, A.; Wu, Q.; Ortland, D.; Yoshikawa, A.; Adimula, I.; Rabiu, A.; Kunitake, M.; Tsugawa, T. Ground magnetic effects of the equatorial electrojet simulated by the TIE-GCM driven by TIMED satellite data. *J. Geophys. Res.* **2014**, *118*, 3150–3161. [CrossRef]
12. Wang, J.; Zuo, X.; Sun, Y.-Y.; Yu, T.; Wang, Y.; Qiu, L.; Mao, T.; Yan, X.; Yang, N.; Yifan, Q.; et al. Multilayered sporadic-E response to the annular solar eclipse on June 21, 2020. *Space Weather* **2021**, *19*, e2020SW002643. [CrossRef]
13. Manoj, C.S.M.; Maus, S.; Lühr, H.; Alken, P. Penetration characteristics of the interplanetary electric field to the daytime equatorial ionosphere. *J. Geophys. Res.* **2008**, *113*. [CrossRef]
14. Zhang, K.; Wang, H.; Yamazaki, Y.; Xiong, C. Effects of Subauroral Polarization Streams on the Equatorial Electrojet During the Geomagnetic Storm on June 1, 2013. *J. Geophys. Res.* **2021**, *126*, e2021JA029681. [CrossRef]
15. Ecklund, W.L.; Carter, D.A.; Balsley, B.B. Gradient drift irregularities in middle latitude sporadic E. *J. Geophys. Res.* **1981**, *86*, 8–862.
16. Yan, C.; Chen, G.; Wang, Z.; Zhang, M.; Zhang, S.; Li, Y.; Huang, K.; Gong, W.; He, Z. Statistical characteristics of the low-latitude E-region irregularities observed by the HCOPAR in south China. *J. Geophys. Res.* **2021**, *126*, e2021JA029972. [CrossRef]
17. Wakabayashi, M.; Ono, T. Multi-layer structure of mid-latitude sporadic-e observed during the SEEK-2 campaign. *Ann. Geophys.* **2005**, *23*, 2347–2355. [CrossRef]
18. Reinisch, B.W.; Galkin, I.A.; Khmyrov, G.M.; Kozlov, A.V.; Bibl, K.; Lisysyan, I.A.; Cheney, G.P.; Huang, X.; Kitrosser, D.F.; Paznukhov, V.V.; et al. New Digisonde for research and monitoring applications. *Rad. Sci.* **2009**, *44*, 1 (RS0A24). [CrossRef]
19. Reddy, C.A.; Rao, M. On the physical significance of the Es parameters fbEs, fEs, and foEs. *J. Geophys. Res.* **1968**, *73*, 215–224. [CrossRef]
20. Resende, L.C.A.; Batista, I.S.; Denardini, C.M.; Batista, P.P.; Carrasco, A.J.; Andrioli, V.F.; Moro, J. Simulations of blanketing sporadic E-layer over the Brazilian sector driven by tidal winds. *J. Atmos. Terr. Phys.* **2017**, *154*, 104–114. [CrossRef]
21. Resende, L.C.A.; Batista, I.S.; Denardini, C.M.; Batista, P.P.; Carrasco, A.J.; Andrioli, V.F.; Moro, J. The influence of tidal winds in the formation of blanketing sporadic E-layer over equatorial Brazilian region. *J. Atmos. Terr. Phys.* **2017**, *171*, 64–67. [CrossRef]
22. Carrasco, A.J.; Batista, I.S.; Abdu, M.A. Simulation of the sporadic E layer response to pre-reversal associated evening vertical electric field enhancement near dip equator. *J. Geophys. Res.* **2007**, *112*, 324–335.
23. Hagan, M.E.; Forbes, J.M. Migrating and nonmigrating diurnal tides in the middle and upper atmosphere excited by tropospheric latent heat release. *J. Geophys. Res.* **2002**, *107*, 4754. [CrossRef]
24. Hagan, M.E.; Forbes, J.M. Migrating and nonmigrating semidiurnal tides in the upper atmosphere excited by tropospheric latent heat release. *J. Geophys. Res.* **2003**, *108*, 1062. [CrossRef]
25. Wickert, J.; Michalak, G.; Schmidt, T.; Beyerle, G.; Cheng, C.Z.; Healy, S.B.; Heise, S.; Huang, C.Y.; Jakowski, N.; Kohler, W.; et al. GPS radio occultation: Results from CHAMP, GRACE and FORMOSAT-3/COSMIC. *Terr. Atmos. Ocean. Sci.* **2009**, *20*, 35–50. [CrossRef]
26. Arras, C.; Jacobi, C.; Wickert, J. Semidiurnal tidal signature in sporadic E occurrence rates derived from GPS radio occultation measurements at higher midlatitudes. *Ann. Geophys.* **2009**, *27*, 2555–2563. [CrossRef]
27. Wu, D.L.; Ao, C.O.; Hajj, G.A.; de la Torre Juarez, M.; Mannucci, A.J. Sporadic E morphology from GPS CHAMP radio occultation. *J. Geophys. Res.* **2005**, *110*, A01306.
28. Arras, C.; Wickert, J. Estimation of ionospheric sporadic E intensities from GPS radio occultation measurements. *J. Atmos. Terr. Phys.* **2017**, *171*, 60–63. [CrossRef]
29. Stone, E.C.; Frandsen, A.M.; Mewaldt, R.A.; Christian, E.R.; Margolies, D.; Ormes, J.F.; Snow, F. The advanced Composition Explorer. *Spa Sci. Rev.* **1998**, *86*, 1–22. [CrossRef]
30. Gonzalez, W.D.; Joselyn, J.A.; Kamide, Y.; Kroehl, H.W.; Rostoker, G.; Tsurutani, B.T.; Vasyliunas, V.M. What is a magnetic storm? *J. Geophys. Res.* **1994**, *99 (A4)*, 5771–5792. [CrossRef]
31. Guyer, S.; Can, Z. Solar Flare Effects on the Ionosphere. In Proceedings of the 2013 6th International Conference on Recent Advances in Space Technologies (RAST), Istanbul, Turkey, 12–14 June 2013; pp. 729–733.
32. Tsurutani, B.T.; Verkhoglyadova, O.P.; Mannucci, A.J.; Lakhina, G.S.; Li, G.; Zank, G.P. A brief review of "solar flare effects" on the ionosphere. *Radio Sci.* **2009**, *44*, RS0A17. [CrossRef]
33. Sahai, Y.; Becker-Guedes, F.; Fagundes, P.R.; Lima, W.L.C.; de Abreu, A.J.; Guarnieri, F.L.; Candido, C.M.N.; Pillat, V.G. Unusual ionospheric effects observed during the intense 28 October 2003 solar flare in the Brazilian sector. *Ann. Geophys.* **2006**, *25*, 2497. [CrossRef]
34. Denardini, C.M.; Resende, L.C.A.; Moro, J.; Chen, S.S. Occurrence of the blanketing sporadic E layer during the recovery phase of the October 2003 superstorm. *Earth Space Sci.* **2016**, *68*, 80. [CrossRef]

35. Santos, A.M.; Batista, I.S.; Abdu, M.A.; Sobral, J.H.; Souza, J.R.; Brum, C.G.M. Climatology of intermediate descending layers (or 150 km echoes) over the equatorial and low-latitude regions of Brazil during the deep solar minimum of 2009. *Ann. Geophys.* **2020**, *37*, 1005–1024. [CrossRef]
36. Conceição-Santos, F.; Muella, M.T.A.H.; Resende, L.C.A.; Fagundes, P.R.; Andrioli, V.F.; Batista, P.P. Occurrence and Modeling Examination of Sporadic-E Layers in the Region of the South America (Atlantic) Magnetic Anomaly. *J. Geophys. Res.* **2019**, *124*, 9676–9694. [CrossRef]
37. Jacobi, C.; Arras, C.; Geißler, C.; Lilienthal, F. Quarterdiurnal signature in sporadic E occurrence rates and comparison with neutral wind shear. *Ann. Geophys.* **2019**, *37*, 273–288. [CrossRef]
38. Resende, L.C.A.; Shi, J.; Denardini, C.M.; Batista, I.S.; Nogueira, P.A.B.; Arras, C.; Andrioli, V.F.; Moro, J.; Da Silva, L.A.; Carrasco, A.J.; et al. The influence of disturbance dynamo electric field in the formation of strong sporadic E layers over Boa Vista, a low-latitude station in the American sector. *J. Geophys. Res.* **2020**, *125*, e2019JA027519. [CrossRef]
39. Moro, J.; Xu, J.; Denardini, C.M.; Resende, L.C.A.; Da Silva, L.A.; Chen, S.S.; Carrasco, A.J.; Liu, Z.; Wang, C.; Schuch, N.J. Different Sporadic-E (Es) Layer Types Development During the August 2018 Geomagnetic Storm: Evidence of Auroral Type (Esa) over the SAMA Region. *J. Geophys. Res.* **2020**, *127*, e2021JA029701. [CrossRef]
40. Piggott, W.; Rawer, K. *Handbook of Ionogram Interpretation and Reduction*; US Department of Commerce, Ed.; National Academy of Sciences: Washington, DC, USA, 1972; p. 352.
41. Batista, I.S.; Diogo, E.M.; Souza, J.R.; Abdu, M.A.; Bailey, G.J. Equatorial Ionization Anomaly: The Role of Thermospheric Winds and the Effects of the Geomagnetic Field Secular Variation. In *Aeronomy of the Earth's Atmosphere and Ionosphere*; Springer: Dordrecht, The Netherlands, 2011; pp. 317–328.
42. Abdu, M.A.; Batista, I.S.; MacDougall, J.; Sobral, J.H.A.; Muralikrishna, P. Permanent changes in sporadic E layers over Fortaleza, Brazil. *Adv. Spa. Res.* **1997**, *20*, 2165–2168. [CrossRef]
43. Bulusu, J.; Archana, R.; Arora, K.; Nelapatla, P.; Nagarajan, N. Effect of Disturbance Electric Fields on Equatorial Electrojet Over Indian Longitudes: Ionospheric Disturbance Electric Field. *J. Geophys. Res.* **2018**, *123*, 5894–5916. [CrossRef]
44. Wang, H.; Hermann, L.; Zheng, Z.; Kedeng, Z. Dependence of the Equatorial Electrojet on Auroral Activity and In Situ Solar Insulation. *J. Geophys. Res.* **2019**, *124*, 10659–10673. [CrossRef]
45. Cohen, R.; Calvert, W.; Bowles, K.L. On nature of equatorial slant sporadic E. *J. Geophys. Res.* **1962**, *67*, 965–975. [CrossRef]
46. Didebulidze, G.G.; Dalakishvili, G.; Todua, M. Formation of Multilayered Sporadic E under an Influence of Atmospheric Gravity Waves (AGWs). *Atmosphere* **2020**, *11*, 653–675. [CrossRef]
47. Fritts, D.C.; Alexander, J. Gravity wave dynamics and effects in the middle atmosphere, *Rev. Geoph.* **2003**, *41*, 1–68.